

Estimation of structure , optical and Electrical properties of novel CuInSe_x nanoparticles Vi Hydrothermal method

Aryan A. Omer and Mohanad Q.Kareem

¹Department of Physics, College of Science, University of Kirkuk, Kirkuk, Iraq

drmohanad33@uokirkuk.edu.iq

Article History: Received: 1 August 2021; Revised: 15 August 2021; Accepted: 25 August 2021;

Published online: 31 August 2021

ABSTRACT: In this work, CuInSe nanoparticles were effectively produced using the nanometric technique in this study. The XRD diffraction results showed that it has a monoclinic structure and a hexagonal phase. The expansion of the XRD line of CuInSe is due to the small crystal size. However, with a large number of grid ratios determined by the comparison. The FESEM images confirmed the Se configurations of the agglomerated and circular rectangular nanoparticles. According to the optical properties, it is found that the best energy gap is eV. 1.25 ev ... which helps the thermoelectric performance of materials or sorbents in solar cell applications.

KEYWORD : Hydrothermal Technique , optical properties , electric properties , XRD .

I. INTRODUCTION

Thin film solar cells are considered one of the alternative low-cost solar cells, they have been widely used to convert light energy into electrical energy⁽¹⁾. The quantum confinement effect in nanostructures has sparked interest in a variety of applications. Semiconductor nanoparticles (with a diameter of less than 10 nm and unique size-dependent physical properties) have been studied extensively during the last few decades. The interesting optical features of semiconductor nanoparticles have positioned them as unavoidable energy sources in the future. Photocatalysis, photovoltaics, sensors, photodetectors, and other applications of semiconductor nanoparticles are all being investigated⁽²⁾. In recent decades, renewable energies have emerged as a critical component of electricity generation. Although photovoltaics provide a substantial contribution to this sector, One of the most difficult aspects of maintaining competitive with fossil fuels is lowering costs⁽³⁾. The energy level fluctuates from day to day demand exceeds the pace of growth's upper limit approaches a critical level. The energy used to build new systems is more than the energy transferred to that location by those systems⁽⁴⁾. Land-based photovoltaic (PV) systems generate electricity based PV panel conversion efficiency depends on the area covered by the panels , and sun radiation. PV-generated electricity must contribute significantly to global electricity consumption to have a significant environmental impact. This is only possible if the PV panels are dispersed over a large area. Given a PV panel's lifetime, which is more than 20 years⁽⁵⁾. Ternary and quaternary based chalcogenides have been attracted tremendous scientific and technological interest towards the development of thin film solar cell because of its high absorption coefficient and long mean free path of the charge carriers From chalcogenide family CISE based materials are widely used as absorber for photovoltaic application since its direct

band gap can be tailored from 1.04 eV to 1.68 eV upon the addition of sulfur and/or gallium⁽⁶⁾. The selenium-based thin-film solar cells achieve maximum efficiency amongst the most efficient thin-film solar cells, All these chalcogenide based materials possess bandgap in the range of $E_g = 1.1-1.7$ eV and high absorption coefficients of $\sim 10^4$ cm⁻¹ (7). Nevertheless, the optical analysis of thin-film solar cell materials using spectroscopic ellipsometry (SE) has been rather difficult due to large roughness of samples⁽⁸⁾.

By using CISE nanoparticles with fixed composition and crystalline structures, high temperature selenization processes under a selenium or H₂Se environment can be minimized or even eliminated. Furthermore, the composition of the printed film can be easily controlled on all scales by controlling the composition of the nanoparticles. Several techniques have been reported for the synthesis of CISE and related nanoparticles, such as solvothermal⁽⁹⁾. In the family of multicomponent chalcogenide semiconductors, significant attention has been given to ternary CuInSe₂ (CISE), a promising PV absorber material for thin film solar cells⁽¹⁰⁾.

II. MATERIAL AND METHODS

Preparation : CISE porous structures synthesized by the hydrothermal method. In a typical, the usually prepared solution prepared by dissolving 0.2928 g of Indium chloride in 10 mL DMF water under magnetic stirring for 10 min to get a clear. (2,4,6) wt% selenium (Se) and 10 mL DMF were added to achieve better NaBH₄. Here the adding DMF can be used as a precipitant as well as a medium to help the product achieve the proper shape., a transparent black solution with foam obtained, These solutions were placed in a Teflon-lined stainless steel autoclave with a capacity of 100 mL, which was filled to about half capacity with distilled water. kept at 180°C for 6 hours and then cooled to ambient temperature. To neutralize the solution, the CuInSe_x Thin films were rinsed three times with distilled water and ethanol, and the surrounding water in the product was removed by drying for one hour at 60 degrees Celsius in air.. The technique was performed under comparable conditions to observe the effect of selenium (Se). Finally, the crystal structure, morphology, and optical characteristics will be investigated. CISE was the name of the final product without Se, while CuInSe_x was the name of the product containing Se.

Characterization Details : Continuous scan mode is used to get the X-ray diffraction line profile data ($2\theta = 10-80$) with CuK α ($\lambda = 1.5406$ Å) room-temperature radiation using an X'Pert PRO (PAN analytical) in the Bragg-Brentano diffractometer par focusing the arrangement ($\theta/2\theta$ geometry) (25 C°). The electrons emitted from the cathode filament were driven towards the anode plate using a 40 kV voltage and 30 mA filament current (Cu). The optics of the diffraction beam include Solar slit of 0.04 rad, a fixed diverging slit (0.8709 slit size), a receiving slit with a diameter of 0.100 mm and a scintillator detector To decrease the instrumental contribution to line broadening in XRD, the samples are scanned with a constant step of 0.05 deg of 2θ and a constant counting time of 1.5sec at each level. Under vacuum, field emission scanning electron microscopy was used to analyze particle size and shape (FESEM). Energy dispersive Xray spectroscopy is installed (EDAX). Heat evaporation is used to join aluminum electrodes using the Edward coating unit and an appropriate mask placed on the CISE's surface. High conductivity silver was used to make connections between the aluminum and a few copper wires. Rotation at roughly 90 degrees formed a stainless steel evacuated closed chamber with a regulated hot plate

(10-12 mbar). A multi-pin feed through at the chamber's base provides electrical connections to the heater, thermocouple, and sensor electrodes. The sample was placed on the heater, and the electrical resistance of the sensor was measured with a multimeter.

III. RESULTS AND DISCUSSION

Figure 1 displays the XRD pattern in structural analyses for pure CuInSe and CuInSe_x mixed thin films prepared at (2, 4, 6) % wt Se content by hydrothermal method. As seen in Figure 1, all diffraction peaks of CuInSe are assigned well to the monoclinic structure of a tenorite system. The major peaks are observed for (A) at ($2\theta = 26.2184^\circ, 27.9058^\circ, 29.6948^\circ, 31.7103^\circ, 39.0926^\circ, 41.2145^\circ, 45.1799^\circ, 45.5945^\circ, 51.2987^\circ, 56.5742^\circ$) attributed to the (106), (110), (104), (112), (106), (207), (213), (116), (218), (2014) planes for a tetrahedrite structure. Showing a hexagonal-phase CuInSe_3 formation, which is in agreement with JCDs card No: 00-035-1150, 00-034-1313. The major peaks are observed for (B) at ($2\theta = 21.5320^\circ, 25.4785^\circ, 26.4767^\circ, 26.6866^\circ, 28.8576^\circ, 29.8898^\circ, 31.3182^\circ, 33.5637^\circ, 36.1696^\circ, 38.6949^\circ, 39.4017^\circ, 44.75^\circ$) attributed to the (009), (411), (271), (290), (0012), (116), (114), (1112), (213) planes for a tetrahedrite structure. Showing a hexagonal-phase CuInSe formation, which is in agreement with JCDs card No: 00-035-1150, 00-040-00670. and The major peaks are observed for (C) at ($2\theta = 22.6656^\circ, 24.9555^\circ, 26.5535^\circ, 28.7065^\circ, 30.0079^\circ, 32.0714^\circ, 36.1312^\circ, 39.5437^\circ, 43.9885^\circ, 51.7302^\circ$) attributed to the (112), (403), (510), (114), (116), (203), (703), (500), (752), (905) planes for a tetrahedrite structure. Showing a hexagonal-phase CuInSe formation, which is in agreement with JCDs card No: 00-035-1150, 03-065-4652. Also, the hexagonal structure of In, The three patterns show a Tetragonal structure. The pattern for pure sample shows low crystalline, the second and third pattern at (2,4,6) % wt. Se shows an increase in the intensity of X-ray diffraction peaks, indicating improved crystalline and a larger number of peaks. At half maximum, the Indium oxide peaks appear to be narrower, indicating that the indium oxide crystalline size is growing at this ratio. It's possible that the increased At this ratio, the crystalline size is due to the CuInSex-1 additive's catalysis, which promotes crystal development. In X-ray diffraction, the broadening of the peaks indicates that the size is in the nano range. The Scherer method can be used to estimate the grain size of the particles. It is still used to figure out what the "apparent" domain is widths physical broadening crest profiles since it is a very simple expression.

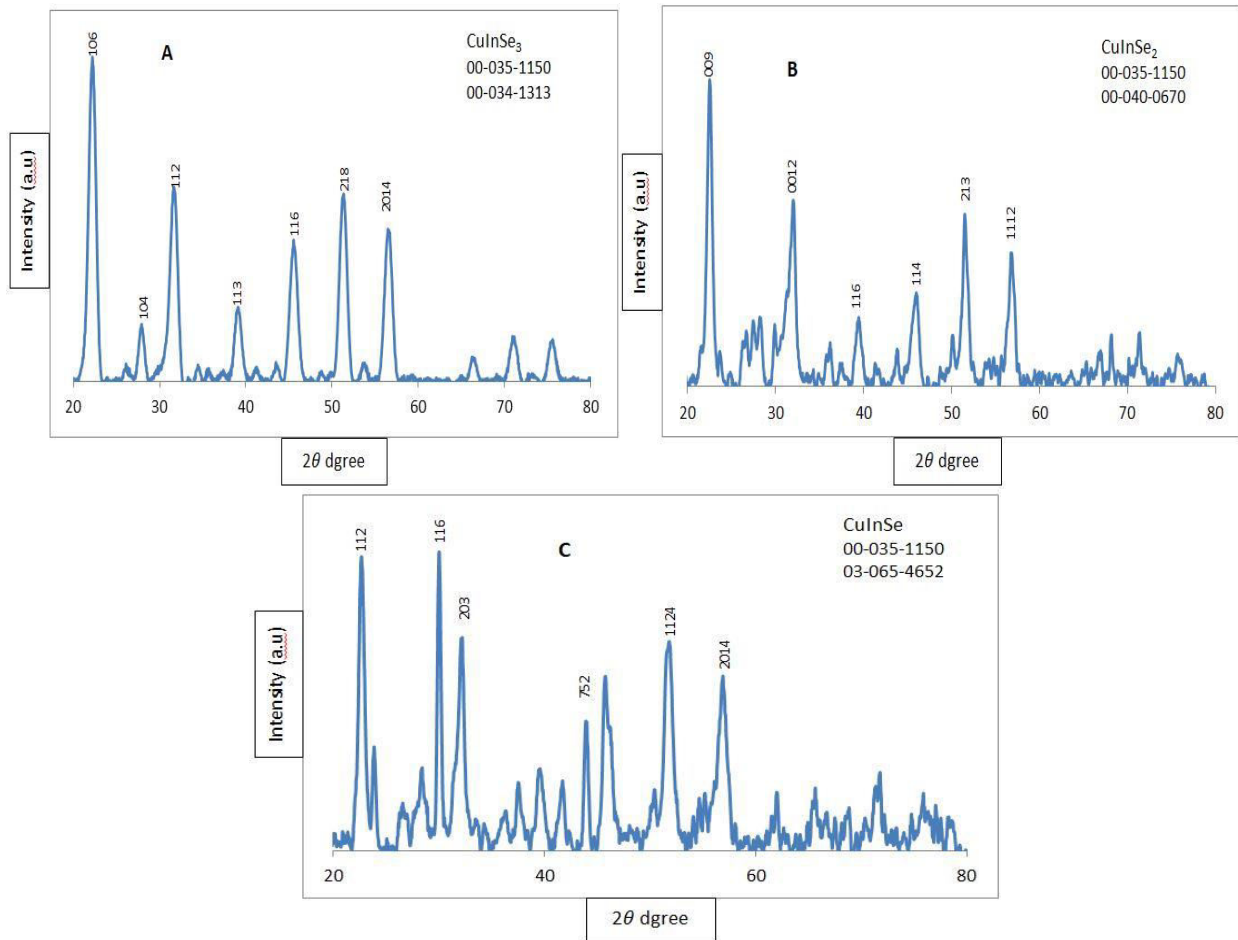


Figure 1: XRD patterns of (A) CuInSe_3 , (B) CuInSe_2 , and (C) CuInSe nanoparticles were deposited on glass surfaces using a hydrothermal technique and then annealed at 180 degrees Celsius.

The mean effect size of the coherently scattering region normal to the reflecting planes is used to determine the crystallite size in this method. The following formula is used to compute the Scherer relationship between crystallite size and integral breadth⁽¹¹⁾:

$$L = \frac{K\lambda}{\beta_L \cos\theta} \quad , \quad \beta_L = \frac{K\lambda}{L \cos\theta} \tag{1}$$

Where L is the appropriate crystallite size in relation to the reflecting plane, K is the form factor (0.9), λ is the wavelength of $\text{CuK}\alpha$ the rays, β is the width of a specific peak's integral, and θ is the angle of diffraction. Size broadening is independent of the order of a reflection, according to Eq. (1). The following equation can be used to calculate the density of dislocation (δ), which The length of dislocation lines per unit volume of the crystal is defined as :

$$\delta = \frac{1}{L^2} \tag{2}$$

Table 1 .Structural parameters, interplanar spacing, crystalline size of pure nanoparticles CuInSe@ (2%) Se

Sample 2 θ	FWHM M [°]	β (rad)	hkl	d_{hkl} (Å)	Scherrer method		standard card
					L_{sh} (nm)	δ (nm) ⁻²	
26.2184	0.96	0.016747	106	2.19	54.514	0.000336	00-035-115000-034-
27.9058	0.90	0.015700	110	2.01	43.986	0.000517	
29.6948	0.72	0.012560	104	1.978	28.525	0.001229	
31.7103	1.02	0.017793	112	1.851	66.371	0.000227	
39.0926	0.72	0.012560	106	1.459	49.002	0.000416	
41.2145	0.96	0.016747	207	1.401	55.508	0.000325	
45.1799	0.48	0.008373	213	1.258	12.223	0.006693	
45.594	0.84	0.014653	116	1.255	62.661	0.000255	
51.2987	1.14	0.019887	218	1.105	41.541	0.000579	
56.5742	1.20	0.020933	201	0.999	43.892	0.000519	

Table 2 .Structural parameters, interplanar spacing, crystalline size of pure nanoparticles CuInSe@ (4%) Se

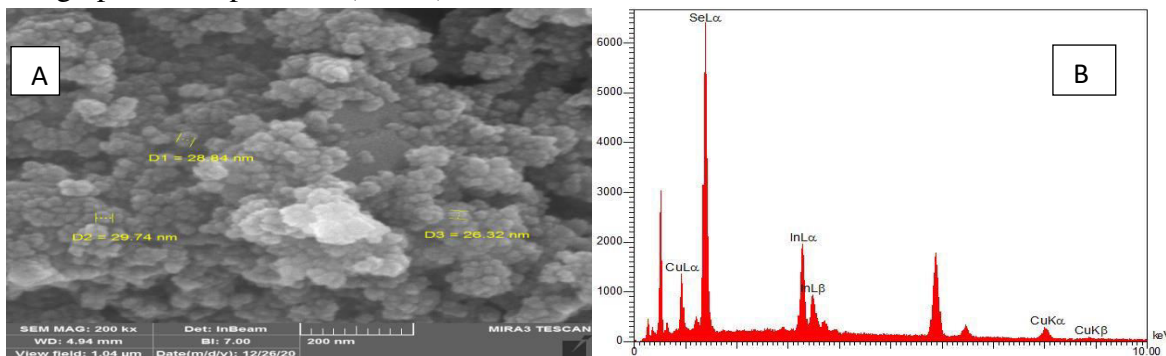
Sample 2 θ	FWHM [°]	β (rad)	hkl	d_{hkl} (Å)	Scherrer method		standard card
					L_{sh} (nm)	δ (nm) ⁻²	
21.532	0.0984	0.001717	009	2.7717	81.4306	0.00015081	00-035-115000-040-
25.4785	0.0984	0.001717	411	2.3181	73.8529	0.00015297	
26.4767	0.3936	0.006866	271	2.1660	65.1727	0.00245732	
26.6866	0.1476	0.002575	290	2.0788	53.7704	0.00034587	
31.3182	0.1968	0.003433	0012	1.8030	39.9084	0.00062787	
33.5637	0.0984	0.001717		1.7250	79.3645	0.00015872	
36.1696	0.2460	0.004291	116	1.5846	31.5194	0.00100657	
38.6949	0.1800	0.003140	114	1.4416	42.7561	0.00054702	
39.4017	0.1800	0.003140	1112	1.4416	42.6627	0.00054942	
44.75	0.1200	0.002093	213	1.2861	62.8553	0.00025311	

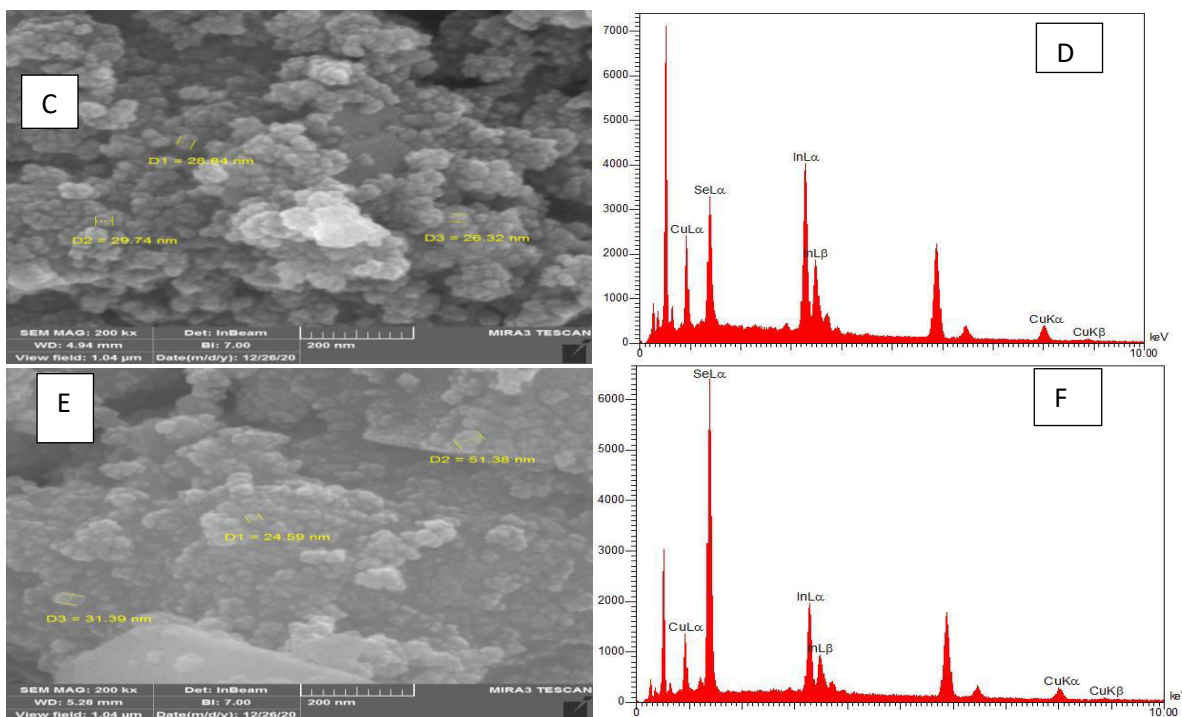
Table 3 .Structural parameters, interplanar spacing, crystalline size of pure nanoparticles CuInSe@ (6%) Se

Sample 2	FWHM [°]	β (rad)	hkl	d_{hkl} (Å)	Scherrer method		standard card
					L_{sh} (nm)	δ (nm)	
22.6656	0.72	0.01256	112	2.642	21.1791	0.002229	00 - 03 5- 11 50 03 - 06
24.9555	0.30	0.00523	403	2.320	26.5464	0.001419	
26.5535	1.20	0.02093	510	2.260	66.1561	0.000228	
28.7065	0.66	0.01151	114	2.015	31.9187	0.000982	
30.0079	1.08	0.01884	116	1.910	72.9505	0.000188	
32.0714	0.78	0.01360	203	1.792	24.0862	0.001724	
36.1312	0.96	0.01674	703	1.517	80.7775	0.000153	
39.5437	1.08	0.01884	500	1.440	71.0730	0.000198	
43.9885	0.60	0.01046	752	1.305	12.6052	0.006294	
51.7302	1.08	0.01884	905	1.124	67.9593	0.000217	

IV.FESEM Analysis

FESEM (field emission scanning microscopy) is a flexible tool for examining material morphology. A tetrahedrite CuInSe structure generated by hydrothermal technique is micrographed nanoparticles (180C°).





Figur 2 . FESEM imeges of CuInSe nanoparticles synthesized hydrothermal method and annealing at 180c^o (A ,C and E) surface morphology (A , C and E) high – resolution image . (B ,D and F) EDX analysis of CuInSe nanoparticles

It offers uniform size distribution with agglomerates , rectangle like structure which in size below 29.74nm were observed . It also confirms that the particles are in the order of nano size. The detailed microstructure of the nanoparticles was further investigated using EDS techniques. EDS analysis of the CuInSe hexahedral nanoparticles as shown in Fig.2 (B ,D and F). Two peaks corresponding to the copper (Cu) peak are observed. located at about 0.9,8 and 8.9 Kev corresponding to L α and K α , K β transitions, respectively. Where are indeum (In) peak appeared at about 3.3 & 3.5 Kev reaching to L α and K β transitions, selenium (Se) peak occurred at about 1.4 Kev corresponding to L α transitions. In addition to height, they were checking the glass substrate, especially for (PEG), and (Na) peaks. The application attached to the examination gadget determined the weight percentage ratio and atomic percentage.

V. Optical Qualities

The film's optical absorption was measured using UV-Vis absorbance spectra in terms of wavelengths (300-1200) nm at ambient temperature, in the visible area and near the infrared region of the electron 2enetic spectrum. Figure 3 demonstrates that the optical absorbance value drops as the wavelength increases. Cu In & Se Film optical absorption coefficient (α) vs photon energy ($h\nu$). The prepared thin film looked to have a light value of $> 10^*$ cm-1. This indicates that straight truncations are permitted. The tuce formale can be used to compute the bandgap energy (Eg)::

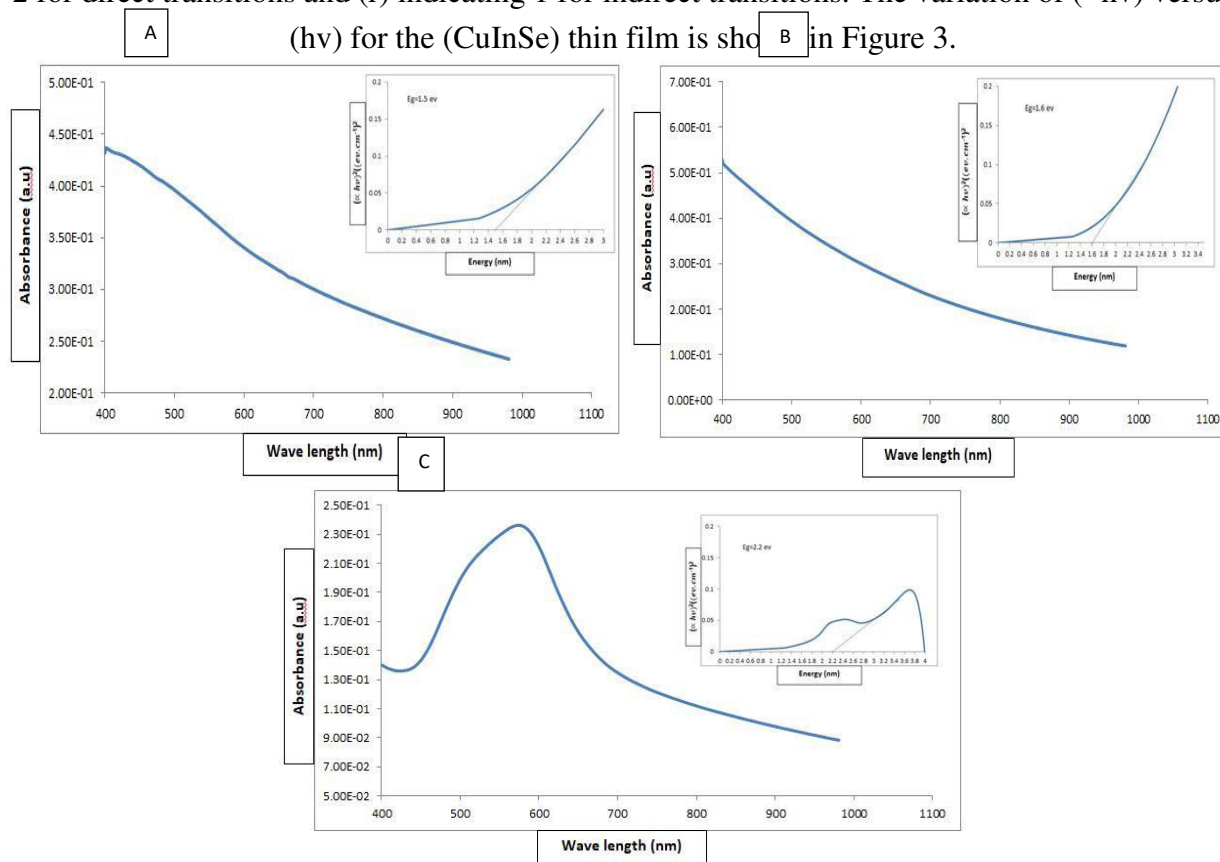
$$B = \frac{(\alpha h\nu)}{(h\nu - E_g)^r}$$

(3)

$$\alpha = B \frac{(h\nu - E_g)^r}{h\nu}$$

(4)

$(h\nu)$ represents the photon energy⁽¹²⁾, while (α) represents the absorption coefficient. The bandgap energy is (E_g) . (CuInSe) has a permitted direct transitions of gap in the optical band $(r=2)$ and (r) is a numerical value that denotes the period of transition type, with (r) representing 2 for direct transitions and (r) indicating 1 for indirect transitions. The variation of $(\alpha h\nu)$ versus $(h\nu)$ for the (CuInSe) thin film is shown in Figure 3.



Figur 3 UV-VIS spectra were used to determine the optical characteristics of the three CuInSe nanoparticles (A, B, and C) as well as the energy gap.

The bandgap energy (E_g) is about A (1.5 ev); B (1.6 ev) ; and C (2.2 ev) the best and near is B for solar cell and photovoltaic applications and thermoelectric materials devices.

VI. The influence of the Hall

The Hall effect is defined as the generation of a a voltage difference across an electrical conductor (the Hall voltage) that is perpendicular to the applied magnetic field and transverse to the current. Edwin Hall is a well-known author It was initially discovered in 1879.. When the specimen is put in the presence of a magnet that is perpendicular to the current flow direction, an electric field E_Y develops across the specimen in a direction that is perpendicular to both the magnetic field and the current. Hall field is the name of this field. The Hall coefficient (R_H)

is calculated by introducing a perpendicular magnetic field B to the electric field, resulting in a current (I). The Hall coefficient is obtained by applying a transverse electric voltage, known as Hall voltage (V_H), across the sample (R_H)⁽¹³⁾.

$$R_H = 1/nq \dots\dots\dots (5)$$

The carrier density is related to the Hall voltage by the equation below, where q is the electron charge and n is the carrier density⁽¹⁴⁾

$$n = \frac{B}{qt} * \frac{I}{V_H} \dots\dots$$

(6)

Where: t a measure of the film's thickness. And the mobility of carriers μ_e or μ_h depends on the kind of the carrier, so for electron or hole, $\mu_{e,h}$ is calculated by⁽¹⁵⁾ :

$$R_H = \frac{\mu_{e,h}}{\sigma_{e,h}} \dots\dots\dots$$

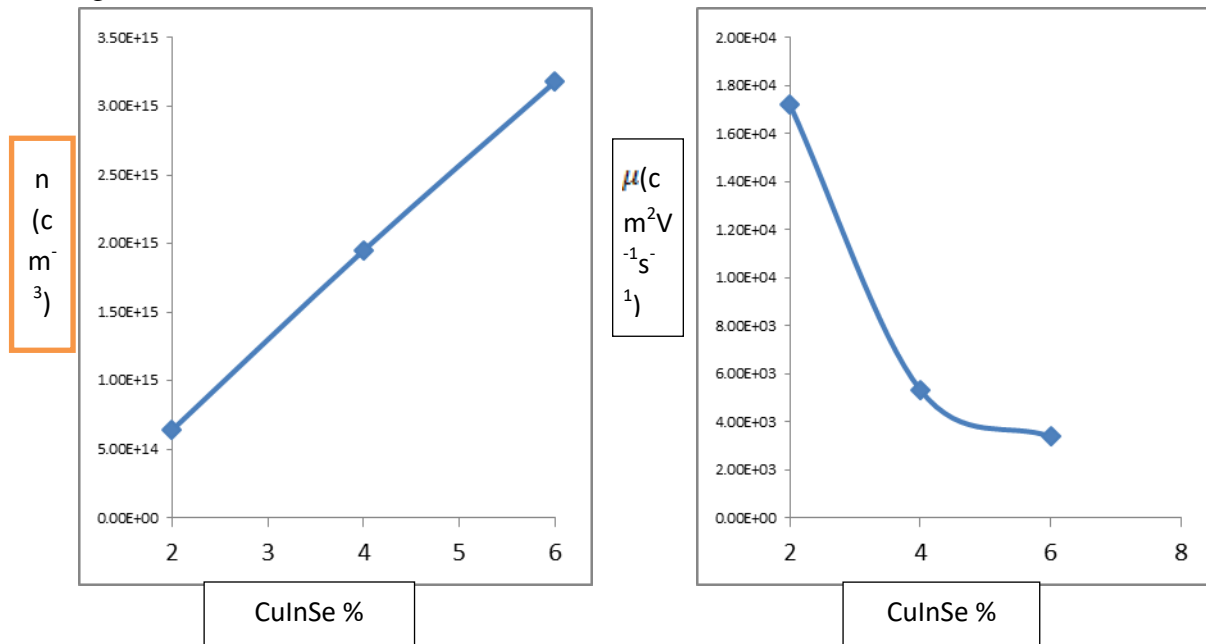
(7)

Where

$$\sigma_{e,h} = nq\mu_{e,h} \dots\dots\dots$$

(8)

The sign of Hall coefficient (R_H) determines the type of semiconductor under investigation.



Fig(4) The graph shows (A) Variation of carrier concentration (n) with a dopant ratio of Se@(2,4 and 6)%wt. CuInSe_x thin films at temperature 180°C. (B) Variation of Mobility (uH) with the dopant ratio of Se@(2,4, and 6)%wt. CuInSe_x thin films at temperature 180°C.

Hall measurements show that all of these thin films have positive Hall modulus (p-type charge carriers). He. She It is attributed to the following two reasons⁽¹⁶⁾

1- The number of electrons is exciting above the conduction bands is larger than the number of holes is stimulating below the valance band.

2- The lifetime of free electrons is boosting from a negative defect state is higher than the lifetime of negative defect state free holes is exciting from a positive defect state

CuInSe _x %	R _H (cm ³ C ⁻¹)	σ (o.cm) ⁻¹	n (cm ⁻³)	μ(cm ² V ⁻¹ s ⁻¹)
2	9.75E+03	1.77E+00	6.40E+14	1.72E+04
4	3.19E+03	1.67E+00	1.95E+15	5.33E+03
6	1.96E+03	1.73E+00	3.18E+15	3.39E+03

Table (4) The result of Hall experiment for CuInSe thin films

The structure of the thin film was changed upon addition of Se, As a result, it could be inextricably connected to a growth in size of a very thin film grains, whereas in C1, the conductivity decreases with an increase in C. This behavior can be explained according to what is given in ref⁽¹⁷⁾, that the structure of the thin film was changed to reduce the volume of Grain and increase the barrier potential of the inner grains making capture vectors change in grain wrapping then increase dispersion. The film gives p-type conductivity up to C3, and one concludes that these machines are lattice dispersion and grain boundary dispersion and the effect of impurity dispersion on the mobility of thin films.

VII..Conclusion

CuInSe nanoparticles were effectively produced using a nano metria technique in this study The XRD diffraction results show that it has a monoclinic structure and hexagonal-phase. The expansion of the XRD line for CuInSe is due to the small crystal size. However, with a large number of retinal ancestry determined by the comparative . FESEM images confirmed the formations of the Se from the agglomerated rectangular nanoparticles and circular . According to the optical characteristics, it was found that the energy gap of each A. B and C is 1.5 ev. 1.25 ev and 1.4 ev ... which aids the thermoelectric performance of materials or sorbents in solar cell applications.

REFERENCES

- 1) Naoto Hamadaa , Takahito Nishimurab , Jakapan Chantanaa,c,* , Yu Kawanoa , Taizo Masudad , Takashi Minemotoa,* Fabrication of flexible and bifacial Cu(In,Ga)Se2 solar cell with superstratetype structure using a lift-off process, 24 February 2020.
- 2) J. Ram Kumar^{1,2} • S. Ananthakumar¹ • S. Moorthy Babu, Role of phosphine free solvents in structural and morphological properties of CuInSe2 nanoparticles 20 May 2016 Springer Science+Business Media New York 2016
- 3) Berit Heidmann^{a, b, c, *} , Franziska Ringleb^d , Katharina Eylers^d , Sergiu Levenco^c , Jorn Bonse^e , Stefan Andree^e , Jorg Krüger^e , Thomas Unold^c , Torsten Boeck^d , Martha Ch. Lux-Steiner^a , Martina Schmid^{a, b, c,} , Local growth of CuInSe2 micro solar cells for concentrator application ,22 October 2017.

- 4) S.A. Khalate, R.S. Kate, R.J. Deokate* A review on energy economics and the recent research and development in energy and the Cu₂ZnSnS₄ (CZTS) solar cells: A focus towards efficiency , 8 May 2018.
- 5) Muhammad Saifullaha , Kihwan Kima , Rauf Shahzad , Jihye Gwaka , Jun-Sik Choa, Jin-Su Yooa , Jae Ho Yuna,,* , Joo Hyung Parka,* Insertion of the AGS layer at the CIGSe/ITO interface: A way to reduce the formation of the GaOx interfacial phase in CIGSe solar cells, 17 December 2017.
- 6) Muhammad Saifullah^{a, b} , Kihwan Kima , Rauf Shahzad^b , Jihye Gwak^{a,b} , Jun-Sik Cho^{a,b} , Jin-Su Yoo^{a,b} , Jae Ho Yun^{a,b,*} , Joo Hyung Parka,*” Insertion of the AGS layer at the CIGSe/ITO interface: A way to reduce the formation of the GaOx interfacial phase in CIGSe solar cells”. Accepted 17 December 2017.
- 7) Mohan Reddy Pallavolu ^a , Arghya Narayan Banerjee ^{a,*} , Vasudeva Reddy Minnam Reddy ^{b,*} , Sang Woo Joo ^{a,*} , Hasi Rani Barai ^a , Chinho Park ^{b,*}” Status review on the Cu₂SnSe₃ (CTSe) thin films for photovoltaic applications”, Accepted 31 July 2020.
- 8) Hiroyuki Fujiwara Shohei Fujimoto Masato Tamakoshi Masato Kato Hideyuki Kadowaki Tetsuhiko Miyadera Hitoshi Tampo Masayuki Chikamatsu Hajime Shibata” Determination and interpretation of the optical constants for solar cell materials”,2016.
- 9) Zhaoxia Han ^{a,b} , Dawei Zhang ^{a,d,*} , Qinmiao Chen ^a , Ting Mei ^c , Songlin Zhuang ^{a,}” One-pot, rapid synthesis of chalcopyrite CuInSe₂ nanoparticles for low-cost thin film solar cell”, 4 July 2013.
- 10) Dehui Li ^{*} , Jing Yang , Weichen Qi , Qiao Gao,” Tetrahedral CuZnInSe₃ nanocrystals: One-pot synthesis, properties, and solar cell application”, 22 July 2020.
- 11) M. B. Tahir, M. Sagir, and K. Shahzad, “Removal of acetylsalicylate and methyl-theobromine from the aqueous environment using nano-photocatalyst WO₃-TiO₂ @g-C₃N₄ composite,” J. Hazard. Mater., vol. 363, pp. 205–213, 2019.
- 12) 1,Mohanad Q. Kareem, 2,Nadim K. Hassan” Evaluation of Williamson–Hall strain and Electrical properties in WO₃@NaDCC/ITO nanoparticles thin films prepared by Hydrothermal method” September-October 2019 | PP 16-26.
- 13) K.Chopra, “ Thin film phenomena” , Mc Graw-Hill Book Company , NewYork (1969).
- 14) S.I.I.Ican ,M.ZOR,Y.Caglar and M.Caglar " Optical characterization of the CdZn(S_{1-x}Se_x)₂ thin films deposited by spray pyrolysis method " Optical Application , Vol.XXXVI,No.1,pp29-31, (2006).
- 15) E.Lifshitz, L.Bykov, M.Yassen, Z.Chen Esterlit, “ The investigation of donor and acceptor stat in nanoparticles of the layered semiconductor PbI₂” chemical physics lett, 273, pp 38-388, (1997).
- 16) R. Rathika et al., “Effect of 200 MeV Ag 15+ ion beam irradiation at different fluences on WO₃ thin films,” Nucl. Instruments Methods Phys. Res. Sect. B Beam Interact. With Mater. Atoms, vol. 439, no. June 2018, pp. 51–58, 2019.

- 17) Hasham , F.Sh, ,M. N, & Hassan N.P.”The effect of doping on the sturtural and electrical properties of CdS Thin films “ Sci . J. Iraqi Atomic Energy commission \ Vol.2 ,No 2, (2000) .